

# PROCEEDINGS OF SPIE

[SPIDigitalLibrary.org/conference-proceedings-of-spie](https://spiedigitallibrary.org/conference-proceedings-of-spie)

## Pulsed laser damage resistance of nanostructured high reflectors for 355nm

Douglas S. Hobbs, Bruce D. MacLeod, Anthony D. Manni

Douglas S. Hobbs, Bruce D. MacLeod, Anthony D. Manni, "Pulsed laser damage resistance of nanostructured high reflectors for 355nm," Proc. SPIE 10447, Laser-Induced Damage in Optical Materials 2017, 104470W (21 November 2017); doi: 10.1117/12.2280572

**SPIE.**

Event: SPIE Laser Damage, 2017, Boulder, Colorado, United States

# Pulsed laser damage resistance of nano-structured high reflectors for 355nm

Douglas S. Hobbs\*, Bruce D. MacLeod, and Anthony D. Manni  
TelAztec LLC, 15 A Street, Burlington, MA, USA 01803-3404

## ABSTRACT

An investigation into the potential for increased laser damage resistance was made for a random distribution and regular array of nanometer scale surface relief structures integrated with dielectric thin-films to create 355nm wavelength selective high reflectors (HR). First, Random Anti-Reflection (RAR) nanostructures were fabricated in a thick silica cap layer deposited on top of a conventional 30-layer HR stack designed as 45 degree turning mirrors. Surface absorption scans of these RAR nano-texture enhanced HR stacks showed a slight decrease in absorption with no impact on performance, however standardized pulsed laser damage threshold testing found no improvement in damage resistance over non-textured silica-cap HR stacks. Second, polarization and wavelength selective nano-structure resonant (NSR) array filters designed to be embedded within thick high damage resistance silica layers were modeled using rigorous coupled wave analysis. Prototypes were fabricated of one NSR design consisting of a low-aspect ratio grating defined in a fused silica substrate with a single thin layer of hafnium oxide over-coat. The performance of NSR prototypes was limited due to multiple fabrication and testing issues. Initial 355nm wavelength, 5ns pulse, s-on-1 laser damage testing yielded a damage threshold in the 3 to 4 J/cm<sup>2</sup> range, comparable to that obtained for the multi-layer HR stacks. Despite these modest early results, it appears that with further fabrication improvements, nano-structure array resonators embedded within silica layers could yield significant increases in the laser damage resistance of HR optics.

**Keywords:** Nano-Textures, Micro-Structured High Reflectors, Guided Mode Resonant Mirrors, Pulsed LiDT, High Average Power Lasers, Random AR, Surface Structure Resonance, Dielectric Gratings

## 1.0 INTRODUCTION

For most of the development history of mirrors and optics for laser applications, the standard approach to enhancing transmission or reflection, or to add functionality, has involved the deposition of thin film dielectric materials on the optic surfaces. Stacks of alternating material layers create effective anti-reflection (AR), high reflection (HR), and wavelength selective (filter) functions through the constructive and destructive interference effect. In recent years, multi-layer dielectric (MLD) coatings have had difficulty surviving the ever increasing fluence within high power laser systems. Problems such as film absorption, film defects, water inclusion, and electric field enhancement within the stacks, lead to inconsistent performance and unreliable operation, imposing limits on power scaling. An alternative to thin-film stacks for creating AR functionality with none of these limitations involves fabricating arrays of sub-wavelength, nanometer-scale surface relief structures directly in an optic surface<sup>[1-3]</sup>. An AR surface texture inherits the mechanical, chemical, and optical durability of the bulk optic material, creating a graded index function that has been widely demonstrated over the last decade to provide a laser damage resistance many times greater than thin-film AR coatings deposited by any technique<sup>[4-8]</sup>. The development of microstructure-based HR and filter functions with high laser damage resistance has not kept pace with the AR microstructure advances. One approach to HR microstructure design that shares the single material solution of AR microstructures, is to utilize an array of surface relief "Aztec" structures<sup>[9,10]</sup>, but this requires complex and expensive fabrication. Another single material HR approach employs varying porosity silica layers to create a stack of high and low index layers in a traditional MLD HR design<sup>[11,12]</sup>. Such all silica HR stacks have exhibited a laser damage resistance up to four times higher than thin-film HR coatings with thresholds approaching the levels attained by AR microstructures<sup>[12]</sup>. However, as found with porous silica and alumina sol-gel film AR coatings<sup>[7]</sup>, porous silica HR stacks may suffer from short term degradation due to the trapping of environmental contaminants (water, hydrocarbons) within the structure voids. It has been shown that due to the open nature of Random AR nano-textures (RAR) defined in silica substrates,

---

\* [dshobbs@telaztec.com](mailto:dshobbs@telaztec.com); phone 1-781-229-9905; [www.telaztec.com](http://www.telaztec.com)

adsorption of environmental contaminants is avoided leading to long term stability and high damage resistance<sup>[7]</sup>. As part of this study, RAR nano-textures were fabricated within silica cap layers deposited on traditional design MLD HR coatings with the goal of increasing laser damage resistance without compromising long-term stability.

In addition to incorporating silica cap layers and porous silica layers within thin-film HR coating stacks, some success at improving MLD HR laser damage resistance has resulted from modifying the material layers in the HR stack where the highest electric field intensities occur. A preliminary study intended to adapt this design approach to improve the damage resistance of wavelength and polarization selective microstructure resonators, is also part of this work.

## 2.0 HIGH REFLECTOR DESIGNS INCORPORATING NANO-STRUCTURES

### 2.1 Nano-structure enhanced high reflectors, NEHR, 355nm.

The first goal of this study was to create near-UV wavelength mirrors incorporating nanometer scale structures that could be submitted to the 2017 Thin-Film Damage Competition. Conventional MLD HR coatings were designed using the commercial thin film modeling software TFCALC (Software Spectra, Inc., www.sspectra.com) with performance targets set by the Competition. The HR optics were required to have a reflection greater than 99.6% for 355nm wavelength, transverse magnetic (Tm or ‘P’) polarized light incident at a 45° angle (AOI). The stack design was optimized for a >20nm HR bandwidth using 13 pairs of high and low refractive index materials chosen as hafnium oxide (HfO<sub>2</sub>, n=2.01 at 355nm) and silicon dioxide (SiO<sub>2</sub>, n=1.47 at 355nm) with layer thicknesses of 47nm and 56nm, respectively. Fused silica substrates (n=1.47 at 355nm) were modeled along with a 1000nm thick SiO<sub>2</sub> layer on top of the MLD stack. Such a ‘cap’ layer is widely used in the industry to enhance laser damage resistance and stabilize performance particularly for vacuum applications. RAR nano-textures etched in the cap layer were modeled in the thin-film software as a reduced thickness SiO<sub>2</sub> layer topped by a uniform custom material layer with an effective refractive index of 1.2 ( $\sqrt{n_s}$ ) to simulate an idealized single wavelength ¼ wave AR coating. The simulation results given in Figure 1 show no change in target reflection between textured (solid green curve) and non-textured (dotted black curve) cap layer MLD designs, though the out-of-band reflections are substantially reduced due to the broadband nature of RAR nano-textures. Cross sections of the non-textured cap (Control) and

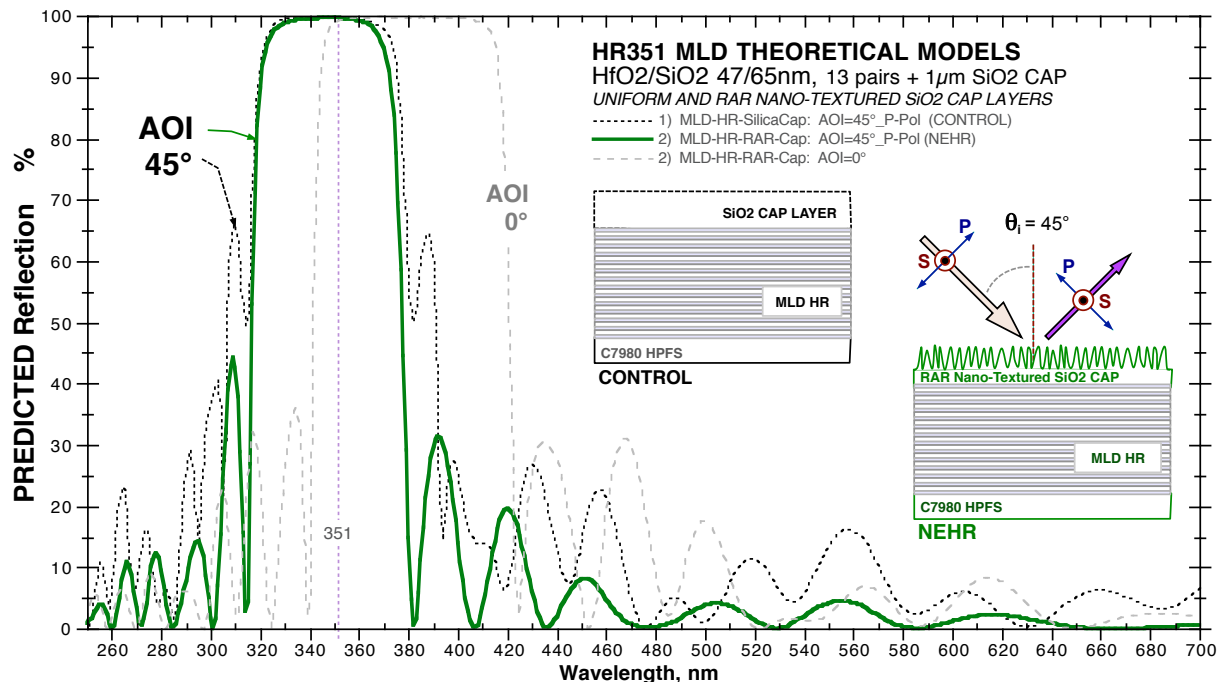


Figure 1: Predicted spectral reflectance of silica-capped HR stacks with (solid green curve) and without (dotted black curve) RAR nano-texturing for light incident at 45 degrees. The dashed grey curve shows the performance for normal incidence light

RAR Nano-texture Enhanced HR (NEHR) design stacks are also shown by the inset diagrams. Note that for this design, the center wavelength of the HR band was shifted to a shorter wavelength at 351nm. This was done so that the target wavelength of 355nm would remain within the HR band for light incident on-axis at 0° (dashed grey curve), allowing the stack performance to be measured on-axis with unpolarized light, and allowing for comparison to other microstructure-based HR designs that operate on normally incident light.

## 2.2 Nano-structure array resonant high reflectors, NSR, 355nm

By defining an array of nanometer-scale features in a dielectric material layer with a higher refractive index than the underlying substrate or surrounding media, a resonance with the transverse electric field of a light wave passing through the array, can be realized<sup>[1,3-15]</sup>. Such nano-structure array resonators (NSR) can be configured to produce a wavelength selective HR function, polarization selective filters, and phase delay elements. A wide body of research exists for NSR devices known variously as photonic crystals, surface structure reflectors<sup>[17]</sup>, meta surfaces<sup>[22]</sup>, and most notably guided mode resonators (GMR)<sup>[16-28]</sup>. In contrast to thick, longitudinally resonant MLD HR film stacks, efficient reflectors and many other unique optical functions can be created with just a single, thin, transversely resonant NSR layer. With this simplified structure and drastically reduced absorption compared to MLD film stacks, such NSR devices have the potential for high laser damage resistance. This potential has yet to be realized possibly due to the early stage of NSR research. The many lessons learned for increasing the damage resistance of thin-film interference coatings, such as the use of silica cap layers and the layer manipulation to reduce the electric field intensity swings internal to the film stack, need to be adapted and applied to NSR technology.

In an initial study of the pulsed laser damage resistance of narrow-band NSRs designed for laser wavelengths ranging from 355nm to 1573nm, tantalum pentoxide (Ta<sub>2</sub>O<sub>5</sub>) and zinc sulfide (ZnS) materials were used for the high index nano-structured layers, and borosilicate glass was used as the substrates<sup>[19]</sup>. Damage thresholds were low for these early prototypes likely due to many factors related to defects and absorption in the materials selected. This work focuses on NSR designs for 355nm laser HR where, as with many MLD HR optics, HfO<sub>2</sub> is chosen as the high refractive index material due to its relatively low absorption and damage resistance. In addition, low index SiO<sub>2</sub> layers are included as caps or to embed the nano-structured HfO<sub>2</sub> layer of the NSR design, an approach that has been successful for increasing damage resistance of MLD mirrors. Another NSR design choice is to pursue a dual function wavelength and polarization selective NSR filter that may have more utility as an output coupler or clean-up polarizer component within a high power UV laser system, and is easier to fabricate due to the simplified one-dimensional grating structure.

To predict the performance of various NSR configurations, a vector diffraction calculation is made using rigorous coupled wave analysis (RCWA) software. A three dimensional unit cell structure is input to the model as a stack of two-dimensional layers where each 2D layer can include multiple material transitions, and the calculation proceeds by solving Maxwell's equations at each layer. Figure 2 shows cross sections of NSR structure options input to the modeling software with a goal of realizing a >99.5% reflection for a wavelength of 355nm (the third harmonic, 3 $\omega$ , of a typical rare-earth doped solid state high power laser such as Nd:YAG). The design space has been constrained by material choices as previously described, and by available fabrication process equipment and limitations. The baseline approach is then to define the NSR grating structure in the surface of a fused silica substrate, then deposit HfO<sub>2</sub> over the grating so that the grating is also replicated in the HfO<sub>2</sub> layer. Last a thick layer of SiO<sub>2</sub> is deposited to encapsulate the grating, and RAR nano-textures are etched part way in the surface to eliminate reflection losses from the SiO<sub>2</sub> cap layer. To avoid diffraction loss from the NSR structure, the structure pitch ( $\Lambda$ ) is set to less than the target wavelength. With the choice of a grating structure, the resonator array is asymmetric and therefore polarization selective, an electric field parallel to the grating lines labeled as 'S', perpendicular labeled as 'P'.

The ratio of the grating line width to the grating pitch – the duty cycle – impacts the spectral shape of the resonance and the level of reflection outside the resonance band. Finally, the depth of the grating structure determines the “order” of the resonance where the lowest order resonance is characterized as a sharp narrow peak as illustrated on the left of Figure 2, and a higher order, broader bandwidth resonance results for deeper structures as illustrated in the right half of Figure 2.

Figure 3 gives a plot of the predicted spectral transmission (solid blue curve) and reflection (solid green curve) for S-polarized light incident on axis (AOI=0°) to the first order NSR grating structure shown in the diagram inset. The structure consists of a 220nm pitch grating with a 130nm line width (0.6 $\Lambda$ ) etched into a fused silica substrate to a depth of 52nm, with a conformal coating of HfO<sub>2</sub> 50nm thick, and a 500nm thick SiO<sub>2</sub> cap with an RAR nano-texture etched 150nm to eliminate reflections from the interface. The resonance shows a single narrow peak at 355nm with an efficiency of 99.9% and a full width half maximum bandwidth (FWHM) of 11nm. A second calculation not shown in the figure for P-polarized light, shows no resonance near 355nm and a reflection loss below 0.1% giving a polarization contrast ratio above 1000:1.

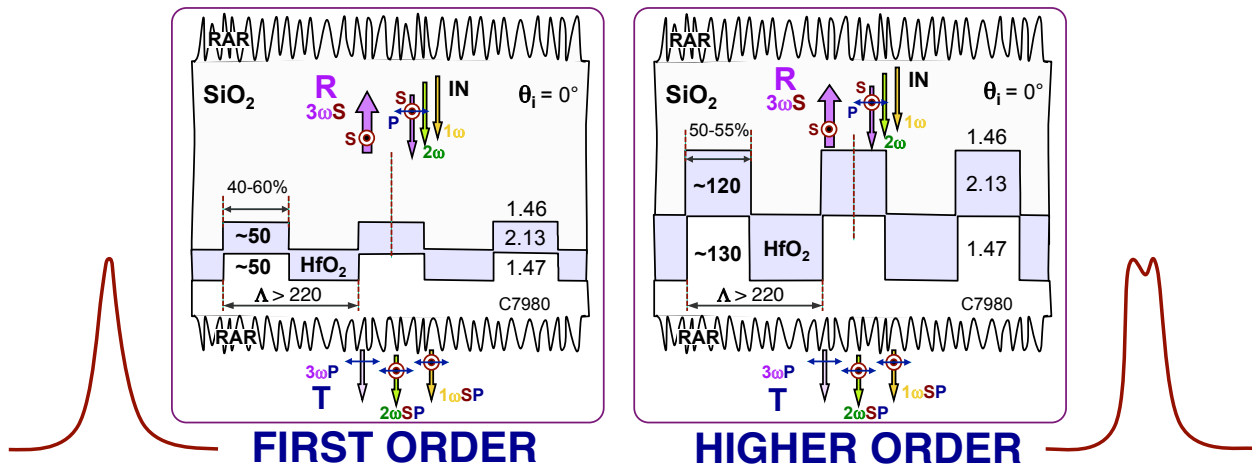


Figure 2: Sub-wavelength first order (left) and higher order (right)  $3\omega$  NSR 1D design concepts.

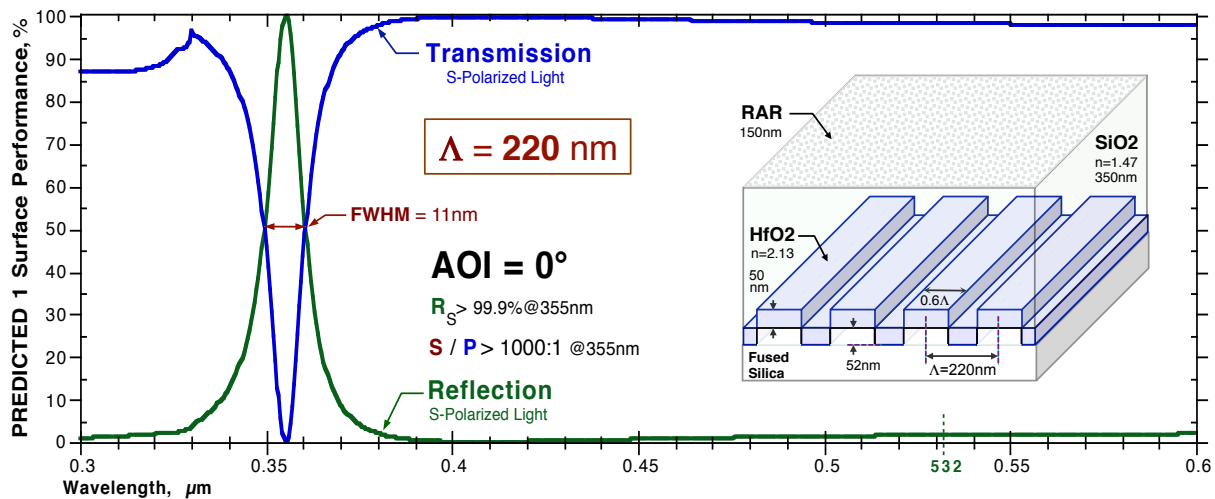


Figure 3: RCWA performance prediction for the 1<sup>st</sup> order  $3\omega$  NSR polarization selective grating shown by the inset diagram.

While the structure of Figure 3 is readily fabricated, and the resonance predicted may be useful as an output coupler or clean-up polarizer, the narrow bandwidth is not suitable for most HR applications. In addition, the shallow grating structure allows too much reflection loss at the longer wave harmonics making it less suitable for filter applications. A broader bandwidth solution with improved AR properties for longer wave harmonics can be attained with a higher aspect ratio – higher order resonance – grating as shown in Figure 4 above. By increasing the thickness of the grating to 135nm, two narrow resonances are supported with slightly displaced peaks yielding a 99.5% reflection bandwidth of about 15nm, a FWHM bandwidth of 38nm. Polarization contrast is slightly reduced to about 800:1. Reflection loss at the first harmonic (not shown, 1064nm,  $1\omega$ ) is improved, but higher loss is predicted for the second harmonic (532nm,  $2\omega$ ).

The Figure 3 and Figure 4 NSR designs operate on normally incident light. For applications requiring larger angles of incidence such as turning mirrors, the NSR pitch must be significantly decreased to maintain the 355nm center wavelength and avoid losses from diffraction. However, decreasing the grating pitch requires more expensive lithography and test equipment, and the fabrication process becomes less practical. An alternative is to explore

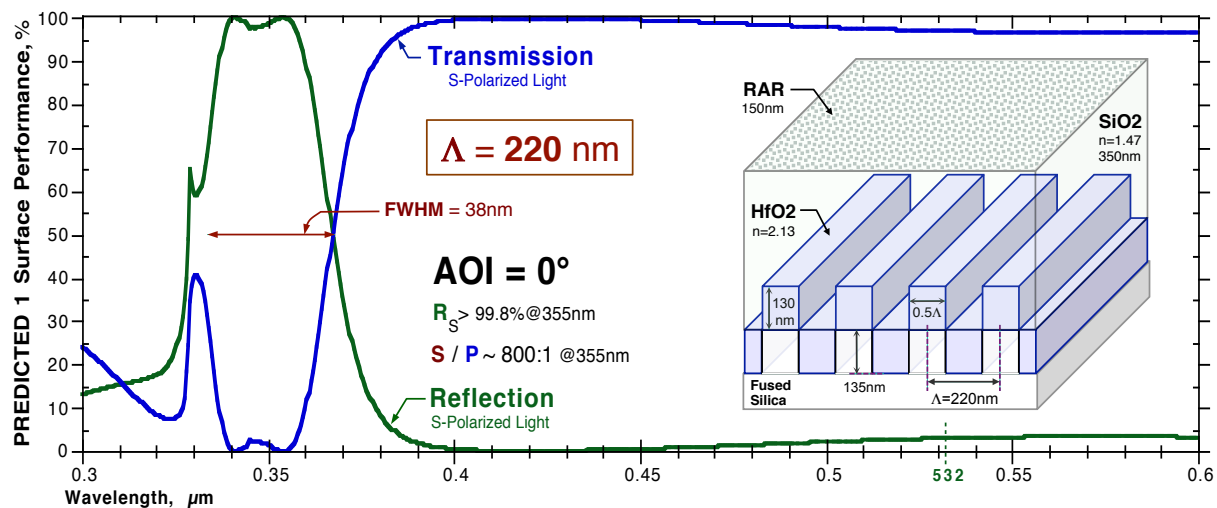


Figure 4: RCWA performance prediction showing increased bandwidth for a higher order  $3\omega$  NSR polarization selective grating.

NSR designs with a grating pitch larger than the target wavelength for ease of fabrication, but adjust the grating shape to minimize the efficiency of free-space propagating diffracted beams that take energy away from the target resonance. Figure 5 shows cross sections of NSR structures with 355nm wavelength resonances at an angle of incidence of 45 degrees. The NSR grating structure on the left in the figure selects for P-polarized light with a grating pitch about 2 times the resonant wavelength of 355nm, while the NSR grating structure in the right diagram selects S-polarized light at a grating pitch about 1.5 times the resonant wavelength. Note the presence of side order diffracted beams indicated by the  $\pm 1R$  and  $\pm 1T$  labels. Second order transmitted diffracted energy ( $\pm 2T$ ), not indicated for simplicity, are allowed by these larger pitch NSR structures, and the number allowed side orders is directly related to the grating pitch.

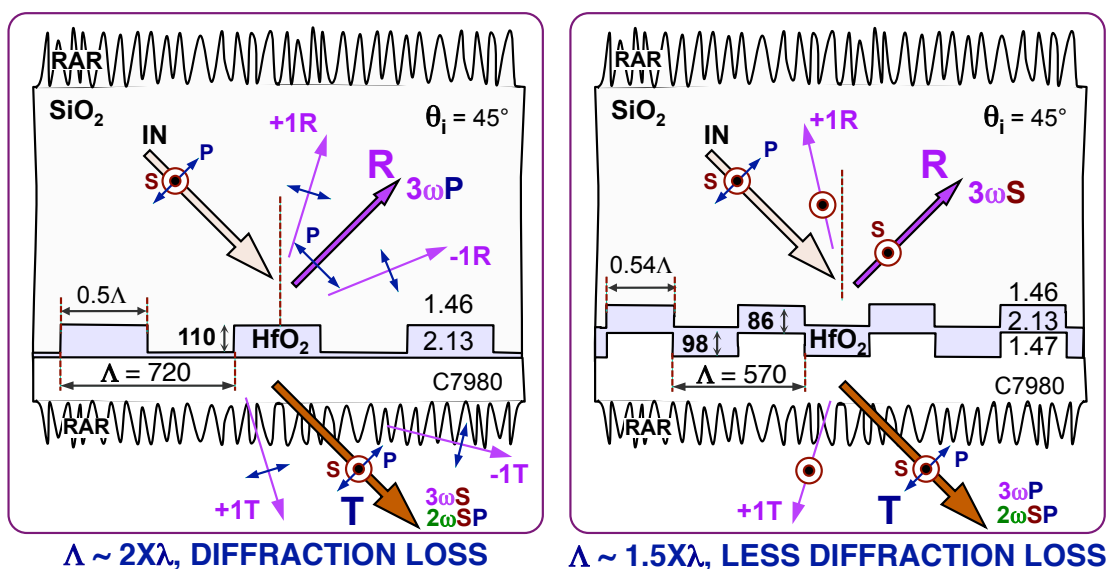


Figure 5: Sub-wavelength first order (left) and higher order (right)  $3\omega$  NSR 1D design concepts.

Figure 6 shows the predicted transmission and reflection of P-polarized light incident at an angle of  $45^\circ$  to the NSR structure shown on the left of Figure 5 and in the diagram on the right in the figure. Also plotted is the reflection of the +1 diffracted beam (dashed light green curve) and the transmission of the +1 diffracted beam (dashed light blue

curve). Along with second order beams not plotted, the total efficiency removed from the target resonance is about 6%. This narrow band filter can be readily fabricated using existing equipment, and although the efficiency is lower than desired, the polarization contrast is high and the reflection loss for higher harmonics is very low. However, total transmission loss for the longer wavelengths can be as high as 10%, making this design less desirable as a dichroic beam splitter.

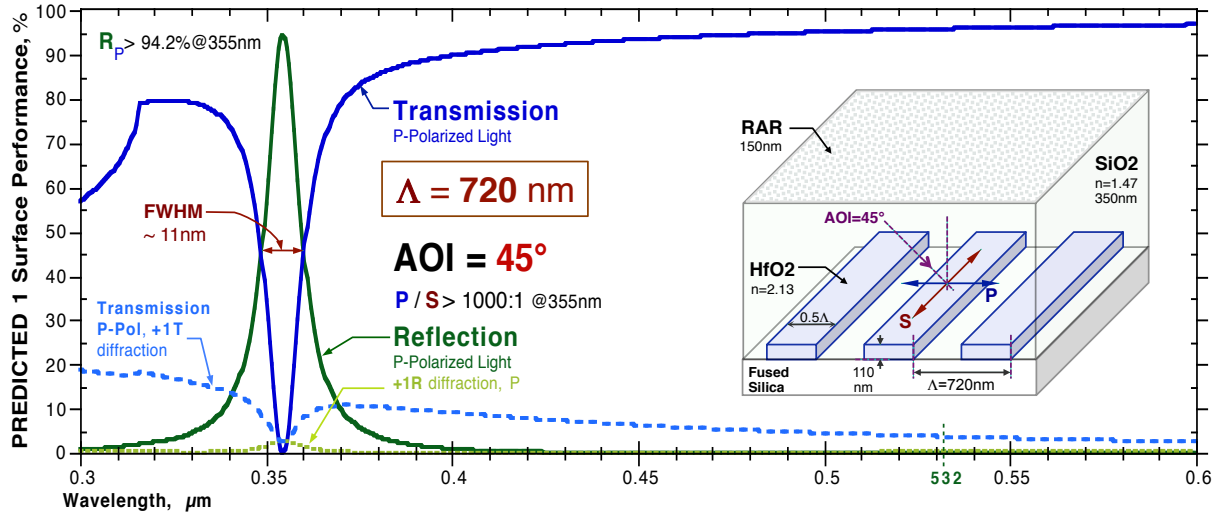


Figure 6: RCWA performance prediction for a 45° AOI 3ω NSR P-polarization selective design with  $\Lambda \gg 3\omega$ .

Reduced losses and a significantly increased bandwidth is predicted for the NSR grating design shown on the right of Figure 5 and as the inset diagram of Figure 7. This design is also quite practical to fabricate and shows extremely low diffraction losses at 355nm, predicting an efficiency over 99% and a FWHM bandwidth of 45nm. Transmission loss for the longer wavelength harmonics is higher than desired mainly due to the energy shifted to the  $\pm 1$  and  $\pm 2$  reflected diffraction orders. In addition, polarization contrast is poor, just 25:1 due to the influence of a closely spaced resonance for P-polarized light. Considering all of these factors, the design of Figure 7 was chosen as the best candidate for the fabrication and damage testing trials described in the following sections.

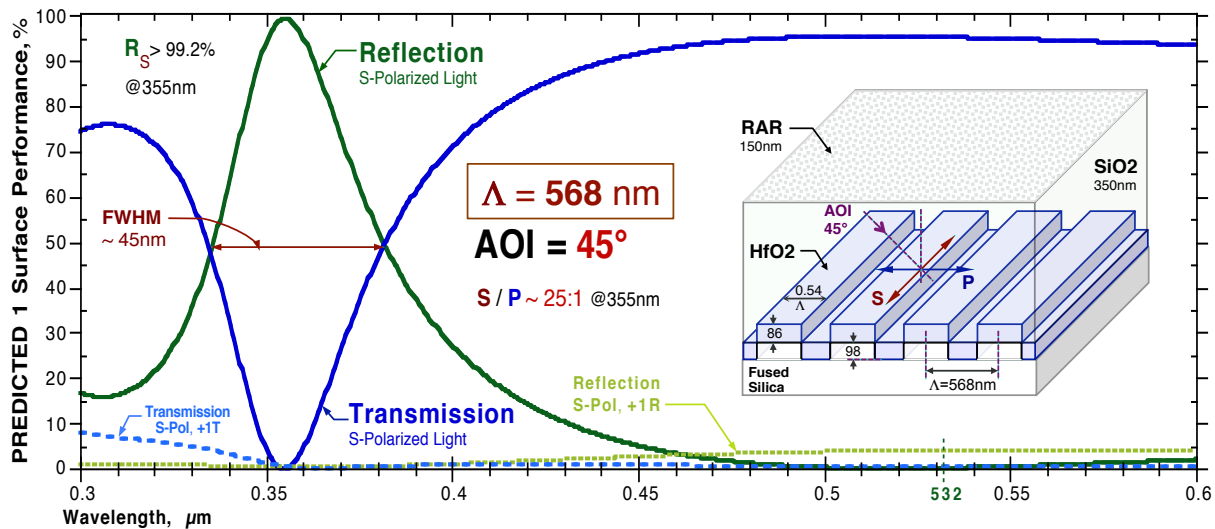


Figure 7: RCWA performance prediction for a 45° AOI 3ω NSR S-polarization selective design with  $\Lambda \sim 1.5 \text{ times } 3\omega$ .



### 3.0 NEHR AND NSR FABRICATION AND MEASURED PERFORMANCE

#### 3.1 Nano-structure enhanced high reflector prototypes.

A MLD HR coating was deposited on laser quality polished round UV fused silica (Corning 7980 Grade 0A) windows by Quality Thin Films, Inc. (QTF, Oldsmar, Florida). The HR design was based on the Figure 1 model, but executed using proprietary methods developed at QTF. The stack consisted of 15 pairs of  $\text{HfO}_2$ - $\text{SiO}_2$  high and low refractive index layers capped by a 1000nm thick  $\text{SiO}_2$  layer, all layers specified for lowest absorption over the near UV wavelength range. Seven 50.8mm diameter, 9.5mm thick windows were coated along with a set of fifteen 25.4mm diameter, 6.35mm thick windows, one fused silica and one silicon window included as mechanical witness samples that could be broken for scanning electron microscope (SEM) analysis of the as-deposited stack.

RAR nano-textures of varying depth were then etched into the silica cap layers of a subset of the windows and the witness window to complete the NEHR prototypes. The witness was broken before and after etching and mounted for SEM analysis. Figure 8 shows images of the RAR nano-texture ~220nm deep on top of ~280nm of un-etched silica, which was fabricated out of an initial cap-layer thickness of 900nm.

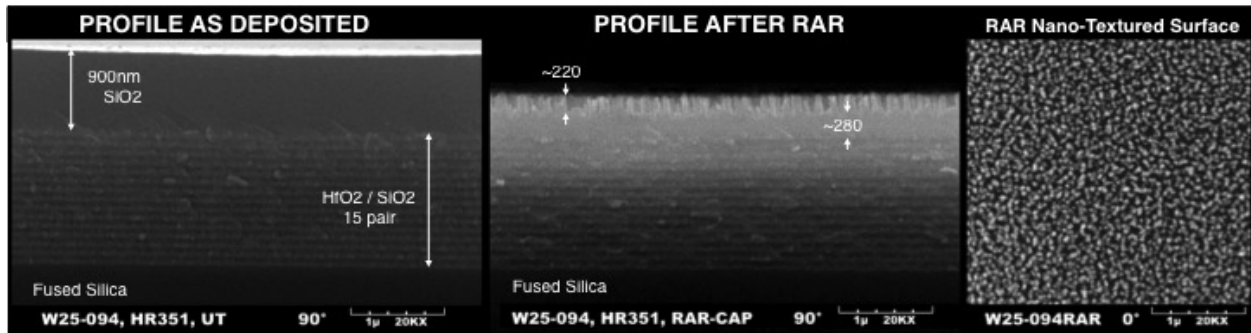


Figure 8: Profile ( $90^\circ$ ) SEM images of a 15 pair  $\text{HfO}_2/\text{SiO}_2$  HR dielectric film stack with a 900nm thick  $\text{SiO}_2$  cap layer before (left) and after (center) RAR nano-texturing of the  $\text{SiO}_2$  cap layer. An overhead ( $0^\circ$ ) view of the RAR nano-texture is on the right.

Two windows, one textured MLD NEHR and one as-received MLD HR to serve as a control sample, were submitted to the 2017 SPIE Laser Damage Competition. Figure 9 shows the measured reflection spectra obtained at  $0^\circ$  AOI by a UV/VIS spectrometer for the Control (dotted black curve) and NEHR (solid green curve) samples. The

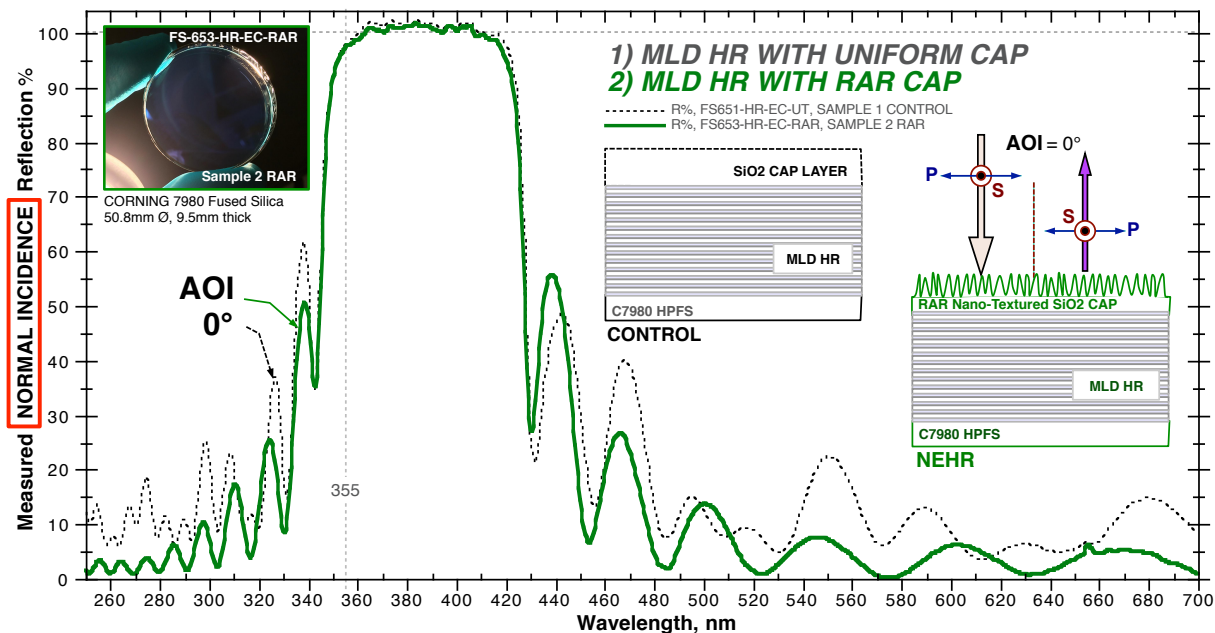


Figure 9: Measured spectral reflectance of silica-capped HR stacks with (solid green curve) and without (dotted black curve) RAR nano-texturing for light at normal incidence, 0 degrees. Two samples submitted to the Damage Competition.



measured performance is nearly identical to the model prediction of Figure 1, showing lower out-of-band reflection and no change in stop-band performance after RAR nano-texture fabrication in the silica cap layer.

A commercially available MLD HR optic specified as >99.6% reflection over the 349-355nm wavelength range, was purchased from CVI Laser (catalog #Y3-1025-0) to include as a comparison sample in the pulsed LiDT tests described below. Figure 10 shows the measured reflection for the CVI MLD HR in comparison to the MLD HR and NEHR film stacks from QTF. The stop-band of the CVI MLD HR was a bit narrower, as it was a different design – the materials and number of layers in the MLD stack were unknown. Note the MLD HR (dotted black curve) and RAR nano-textured NEHR (solid green curve) sample measurements are averaged from four or five separate parts.

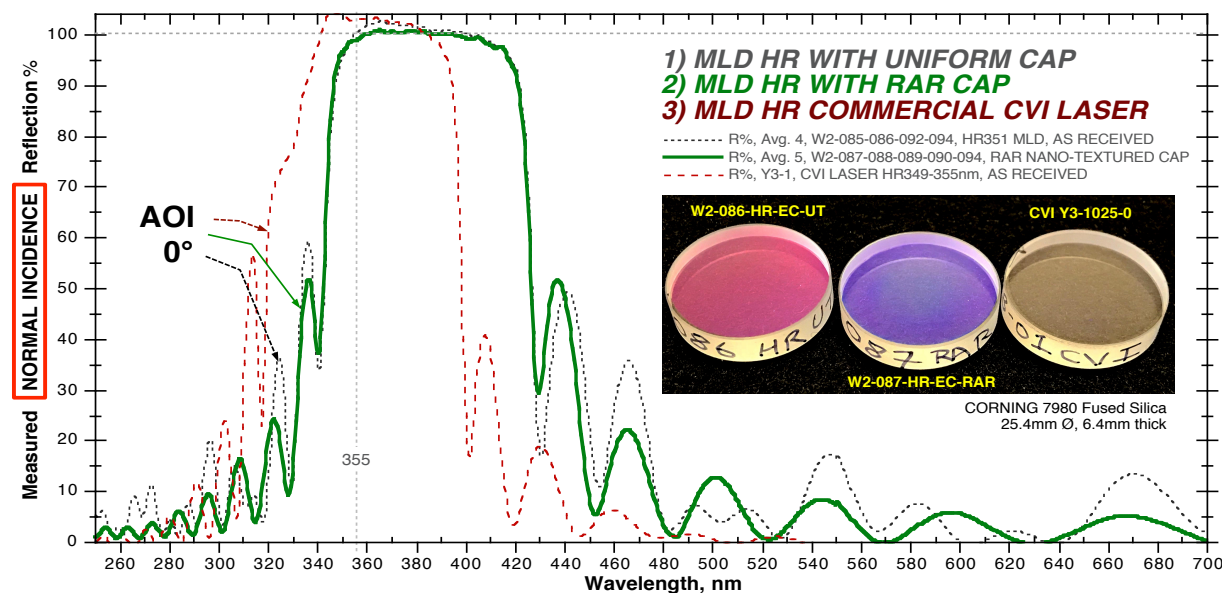


Figure 10: Measured spectral reflectance of silica-capped HR stacks with (solid green curve) and without (dotted black curve) RAR nano-texturing for light at normal incidence, 0 degrees. Twelve samples submitted to pulsed LiDT testing at Quantel.

To evaluate the amount of 355nm laser light absorbed by the MLD HR stacks, and to correlate that absorption level with the pulsed laser damage resistance, the CVI and QTF deposited MLD HR optics were submitted for sensitive Common-Path PhotoThermal Interferometry (CPPI)<sup>[29]</sup> scans conducted by Island Interferometry, a service company spin-off from Stanford PhotoThermal Solutions, Inc. CPPI scans through the bulk, Figure 11, and over the surfaces, Figure 12, show the absorption of the MLD stack compared to the bulk fused silica material, and the absorption

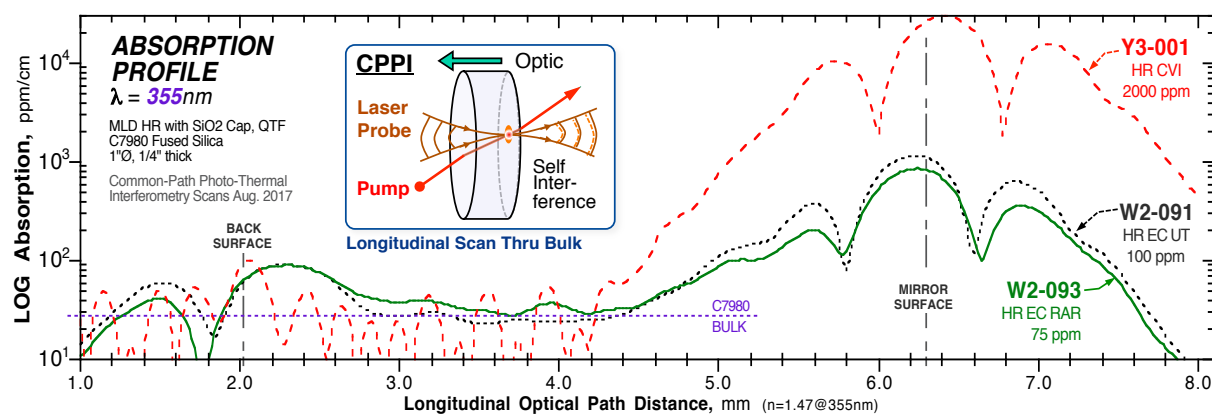


Figure 11: Longitudinal scans giving the surface and bulk absorption of silica-capped HR optics with (solid green curve) and without (dotted black curve) RAR nano-texturing. Absorption of a MLD HR from CVI is also shown (dashed red curve).

uniformity of the MLD surface, respectively. Looking first at the longitudinal scans in Figure 11, the scan shows no surface absorption on the uncoated back surfaces as expected, a bulk absorption in the 20-30 parts per million per cm (ppm/cm) range as indicated by the dashed purple marker, and large spikes in absorption as the scan proceeds across the MLD stack surfaces. Because of the significantly larger absorption observed for the CVI MLD HR (dashed red curve) compared to the MLD HR (dotted black curve) and MLD NEHR (solid green curve) from QTF, the data is plotted on a log scale. The CVI MLD HR surface absorption measures 2000 ppm, 20 times higher than the MLD HR at 100ppm. The fabrication of RAR nano-textures in the silica cap layer of the MLD NEHR sample has the expected effect of reducing absorption to just 75ppm due to material removal.

Figure 12 plots the absorption scans over the surface of the MLD HR stacks to look for absorption spikes due to defects or contaminants. All three samples scanned showed good uniformity over the 3mm long scan distance. Again, the MLD NEHR exhibits the lowest amount of absorption at 73ppm, with the MLD HR and CVI MLD HR average absorption consistent with the Figure 11 scans.

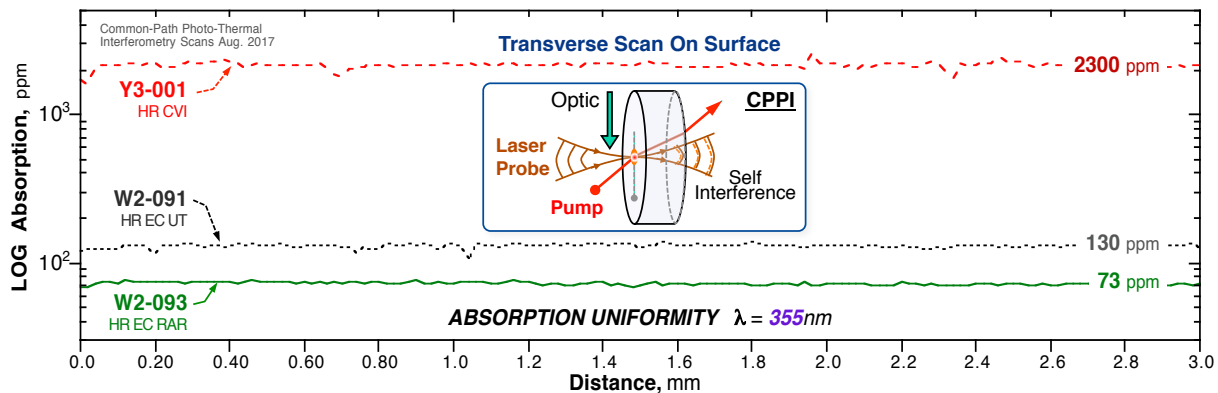


Figure 12: 3mm long transverse scans giving the surface absorption uniformity of silica-capped MLD HR optics with (solid green curve) and without (dotted black curve) RAR nano-texturing. Uniformity for the CVI HR is shown as the dashed red curve.

### 3.2 Nano-structure array resonant high reflector prototypes

Multiple NSR prototypes based on the Figure 7 design were fabricated on laser quality polished fused silica windows (Corning 7980 Grade 0A fused silica, 25.4mm diameter, 4.0mm thick). A three stage process is used involving first the origination of the grating pattern in a photosensitive material coated on the fused silica windows using interference lithography<sup>[21,30]</sup>, followed by transfer of the grating pattern into the fused silica surface via reactive ion etching, then finishing with the deposition of HfO<sub>2</sub> and SiO<sub>2</sub> thin films. SEM imaging and spectrometer

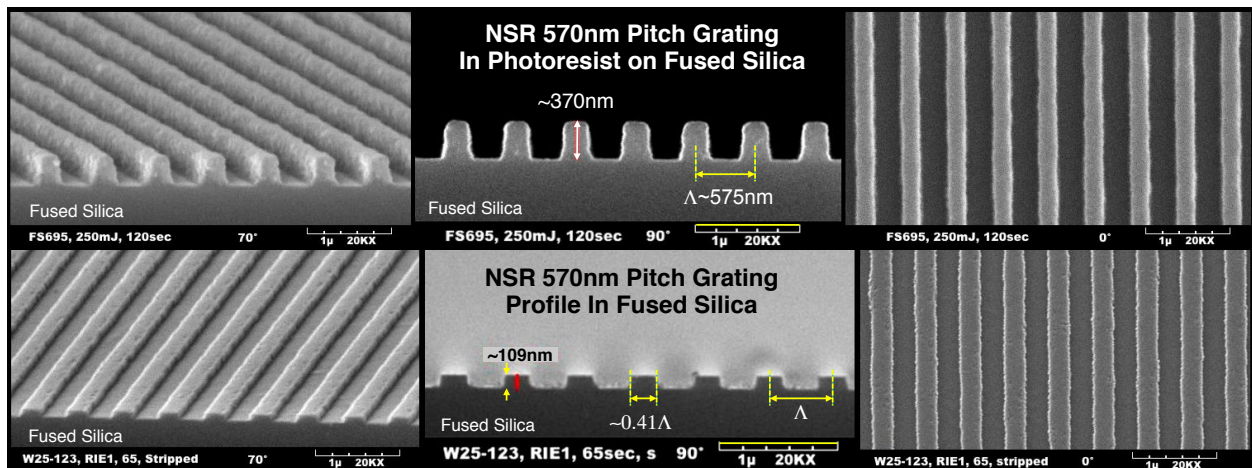


Figure 13: SEM views of the typical NSR grating pattern first originated in a photoresist mask (top row) and after transfer into fused silica surfaces by reactive ion etching (bottom row). Measurements show the grating height, pitch ( $\Lambda$ ), and duty cycle.

reflection measurements are used to provide feedback at each stage of the fabrication process. Figure 13 above shows the first two stages of the fabrication process with SEM views of the grating pattern mask defined in photoresist in the top row, and views of the grating pattern etched into the fused silica surface in the bottom row. The grating pitch measures 575nm by these SEM images, but a more accurate spectrometer measurement records the pattern pitch at 570nm, closer to the target of 568nm. The grating depth and duty cycle were varied between samples in order to bracket the parameters found by the Figure 7 NSR model. The depth and duty cycle for the witness sample broken for the Figure 13 images measured 109nm and 41% respectively, values a bit outside the target values of 98nm and 54%.

A set of fused silica windows with and without NSR gratings were sent to QTF for deposition of the  $\text{HfO}_2$  and  $\text{SiO}_2$  films by ebeam evaporation. Ten windows were coated with 100nm of  $\text{HfO}_2$  only in order to evaluate the  $\text{HfO}_2$  film absorption, deposition uniformity, and conformality to the grating surface. Ten additional windows were coated with 100nm of  $\text{HfO}_2$  and 400nm of  $\text{SiO}_2$ . Measured film thicknesses of the witness windows without an NSR grating were 97nm  $\text{HfO}_2$  and 387nm  $\text{SiO}_2$ . SEM images given in Figure 14 show elevation, profile and overhead views of the  $\text{HfO}_2$  only coating on the grating defined in the fused silica surface (top row), and the two-layer  $\text{HfO}_2$ - $\text{SiO}_2$  coated gratings (bottom row). Looking first at the  $\text{HfO}_2$  coating images, the elevation view ( $70^\circ$ ) shows that in the valleys of the grating the coating is smooth and uniform. The  $\text{HfO}_2$  growth on top of the grating lines appears to have grown in a columnar fashion first from the corners leading to a slight overhang of the valleys and a depression in the center of the lines. The profile view shows that there may exist a slight void in the center of the line, and that the thickness of the coating is greater on top of the lines than in the valleys between (the values greater than 100nm are likely a magnification error). This irregular  $\text{HfO}_2$  growth may have contributed to the growth pattern seen with the subsequent  $\text{SiO}_2$  deposition where the top surface did not planarize as expected leaving a second grating structure with dome shaped lines peaked about 75nm above sharp valleys. A further deviation from the model structure is the small line width that measures just 31% of the grating pitch ( $\Lambda$ ), significantly less than the target duty cycle of 54% ( $0.54\Lambda$ ). The combination of low duty cycle and the overhanging  $\text{HfO}_2$  growth on top of the lines produced the diverging, lateral growth of  $\text{SiO}_2$  on top of the lines, a growth that may have trapped voids at the delta-shaped interfaces above the grating valleys.

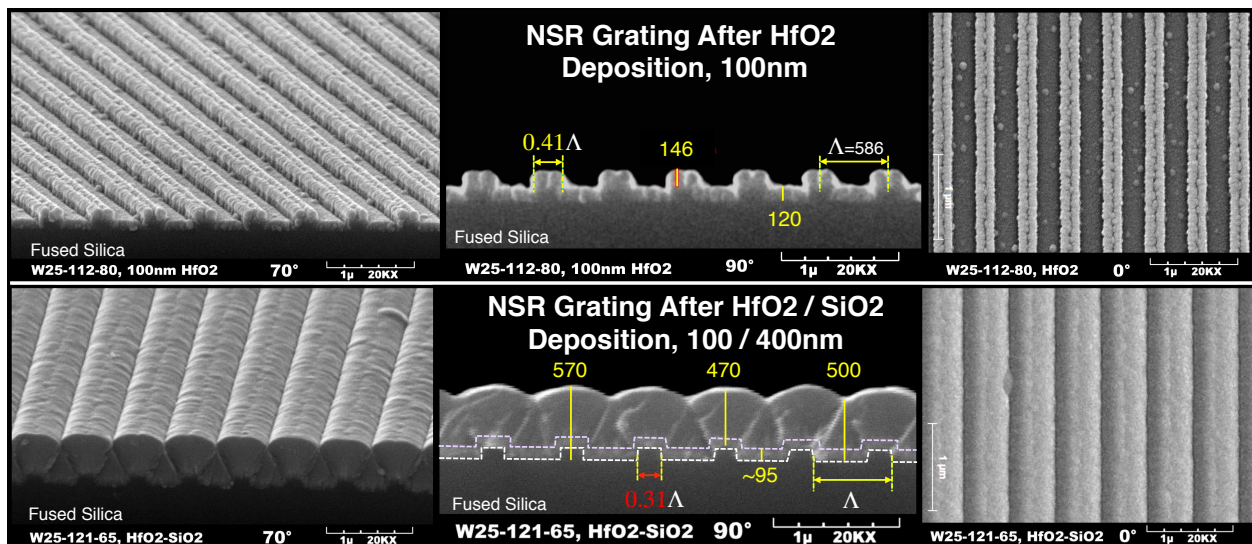


Figure 14: Elevation ( $70^\circ$ ), profile ( $90^\circ$ ), and overhead ( $0^\circ$ ) SEM views of NSR prototypes after deposition of 100nm of  $\text{HfO}_2$  (top row), and after two-layer  $\text{HfO}_2/\text{SiO}_2$  deposition (bottom row). Note the  $\text{HfO}_2$  growth defect on top of the grating lines, and the  $\text{SiO}_2$  top layer is not planar as expected with a duty cycle that measures just  $0.31\Lambda$ , significantly less than the  $0.54\Lambda$  target.

To complete the NSR prototypes, RAR nano-textures were etched into the back surface of the fused silica substrates to eliminate specular reflection loss to a level below 0.1% for broad-band UV through visible band light incident at the design  $45^\circ$  angle. RAR nano-textures were also etched in the top  $\text{SiO}_2$  layers to a depth approximately 125nm so as to also reduce near-UV internal reflections that could effect the target resonance.

A grating based spectrometer (StellarNet Silver-Nova), deuterium-tungsten lamp UV-VIS source (Ocean Optics DH-2000-DUV), two UV transmitting multimode 200 $\mu\text{m}$  core fiber optic cables, and two adjustable focus uncoated fused silica collimating lenses, were configured in a fiber to fiber transmission setup and used to characterize the transmission of the NSR prototypes. For convenience, a thin plate linear polarizer for the near UV wavelength range (Thorlabs LPUV050) was included between the send and receive fibers in the measurement system to allow for user selection of the polarization orientation presented to the sample under test. Rotational stages were used to adjust the incident angle and the NSR grating orientation. Because of the limited performance band of the linear polarizer (>100:1 contrast band 350-405nm), the spectral range for a valid measurement was 330-420nm.

All of the NSR prototypes showed only a weak resonance with low polarization contrast at the target wavelength of 355nm. While measurement system contrast and calibration issues may have contributed in a minor way to the poor results, the dominant factor seems to be the deviation of the as-built NSR structure from the model design, specifically the reduced duty cycle and secondary grating in the SiO<sub>2</sub> layer described above. Figure 15 shows the typical performance of the NSR prototypes where the spectral transmission of S-polarized light oriented parallel to the NSR grating lines and incident at an angle of 45° (solid red curve), is plotted along with the spectral transmission with the linear polarizer rotated 90° to transmit P-polarized light (solid blue curve). The peak resonance is just 25% centered at 360nm, far off the model target of 99% at 355nm shown for reference as the dashed red curve.

From all previous microstructure-based filter work, theoretical model predictions have been in close agreement with the as-built device measured performance<sup>[19,21]</sup>. For the NSR prototypes of this work, the as-built structure deviations shown in Figure 14 and discussed above, were input to the RCWA modeling software to obtain revised performance predictions. First only the large duty cycle variation was varied in the original model structure. While the duty cycle variation has a significant impact on the shape of the resonance and in particular the strength of the diffraction orders, the target resonance efficiency could only be reduced from 99% to 90%, far from the 25% observed. Next the secondary grating formed by the SiO<sub>2</sub> growth pattern, was added to the structure model as a 71nm deep, 84% duty cycle grating on top of a 291nm thick uniform SiO<sub>2</sub> layer. A cross section of the as-built structure model is shown as the inset diagram in Figure 15. Together with a 39% duty cycle and an incident angle of 47°, a very close match to measured performance was obtained for S-polarized light (dotted dark red curve). This model result gives great confidence that by addressing the fabrication issues, high performance can be attained.

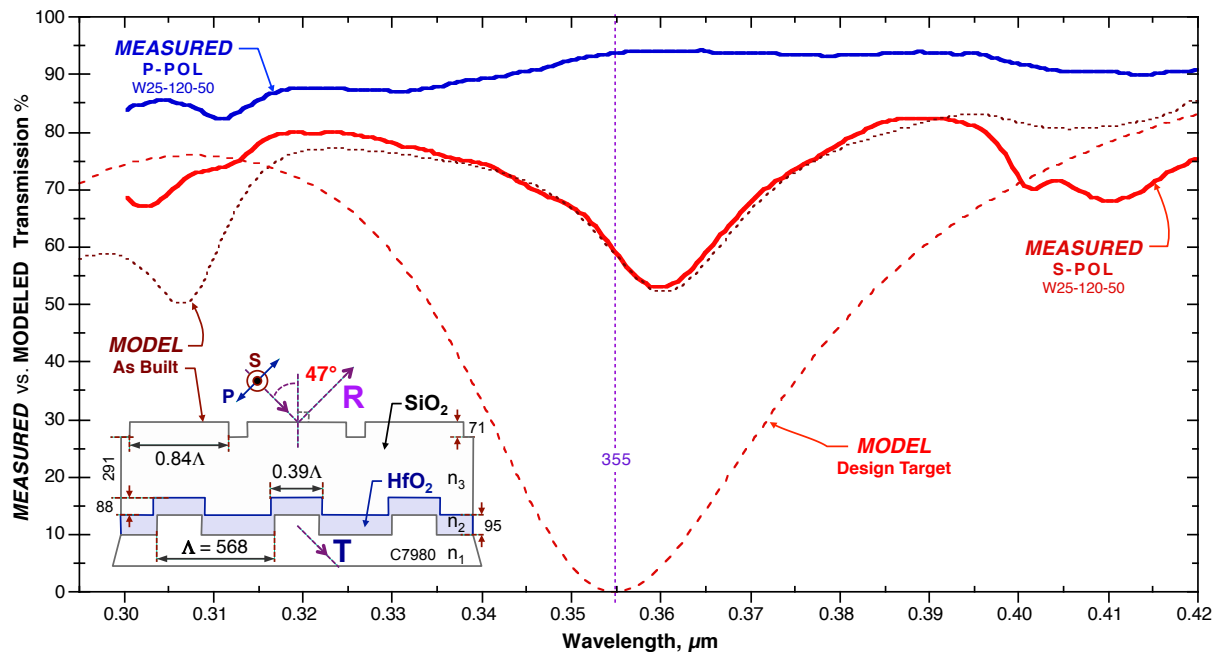


Figure 15: Measured spectral transmittance of linearly polarized light (solid blue and red curves) incident to an NSR filter at a 45° angle. The predicted transmission for S-polarized light from the target structure design (Fig. 5 and dashed light red curve), and the predicted transmission of the as-built structure (inset diagram and dotted dark red curve) are shown for comparison.



#### 4.0 PULSED LASER DAMAGE TESTING, 355nm, 5.8ns

A set of 15 fused silica windows were submitted to Quantel USA in Bozeman Montana for their commercial ‘s-on-1’ type pulsed laser induced damage threshold measurements. “Damage” is defined as any permanent surface change that can be observed at high magnification (150x), and “threshold” is used to describe the lowest fluence required to induce damage at any site. Quantel’s testing adheres to the ISO 11254 standard and involves irradiating a test sample at several different fluence levels, multiple sites per fluence level. The percentage of failures at each fluence is plotted against the fluence levels, to which a least squares linear fit is applied. The 0% damage intercept of the fit determines overall threshold fluence. The specific test configuration was: tripled Nd:YAG laser operating at 355nm wavelength, 5.8ns pulse width (FWHM), 10Hz pulse repetition rate, 0.21-0.35mm focused spot diameters ( $1/e^2$ ), TEM<sub>00</sub> spatial mode, linear polarization, at AOIs of 0° and 45°, ~100 exposure sites on a grid with spacing >2x spot diameter, 150 shots per site, 10 fluence levels. It is common in fused silica and other glasses under test to observe large scale back surface damage, or blow outs. Often this backside damage occurs without damage to the expose surface and is therefore not included in the damage site count. A refinement to the ISO 11254 protocol, ISO 21254, was used for this work where the fluence level increments are adjusted along with an increased number of exposure sites for each fluence level so as to increase the number of damage frequency values above the zero damage threshold and below the 100% damage level, thereby obtaining better linear fits for the reported LiDT.

#### 4.1 Nano-structure enhanced high reflector prototypes.

The LiDT test results acquired by Quantel showed that the RAR nano-textures did not provide any assistance in raising the damage threshold of MLD HR coated optics, and in some cases even lowered it. The scatter plot on the left in Figure 16 gives the damage frequency vs. exposure fluence for MLD HR samples with (RAR CAP) and without (UT CAP) RAR nano-texturing, and for the CVI MLD HR samples. The UT MLD HR, represented with white crosses on the plot, began to damage at 3.6 J/cm<sup>2</sup>, which was similar to the threshold of an RAR-textured HR, represented by green triangles on the plot. The CVI MLD HR sample, represented by red squares, was mistakenly tested with a smaller 0.25mm diameter spot area which may have resulted in the slightly higher LiDT.

The bar graph in the right half of the figure shows the linear fit damage threshold fluences of the various sample types exposed at 0° AOI, and at 45° AOI with P-polarized light. Overall, thresholds at 45° were lower than those at 0°. The two CVI MLD HR samples exhibited thresholds of 4.4 and 4.1 J/cm<sup>2</sup> for a spot diameter of 0.25mm at normal incidence. The highest-performing silica-capped HR at normal incidence was RAR textured and damaged at a threshold of 3.7 J/cm<sup>2</sup> for a spot size of 0.35mm. At 45° AOI, the UT capped HR outperformed all of the RAR-textured HRs, showing no benefit in texturing the top of the MLD with RAR nano-textures despite their lower surface absorption.

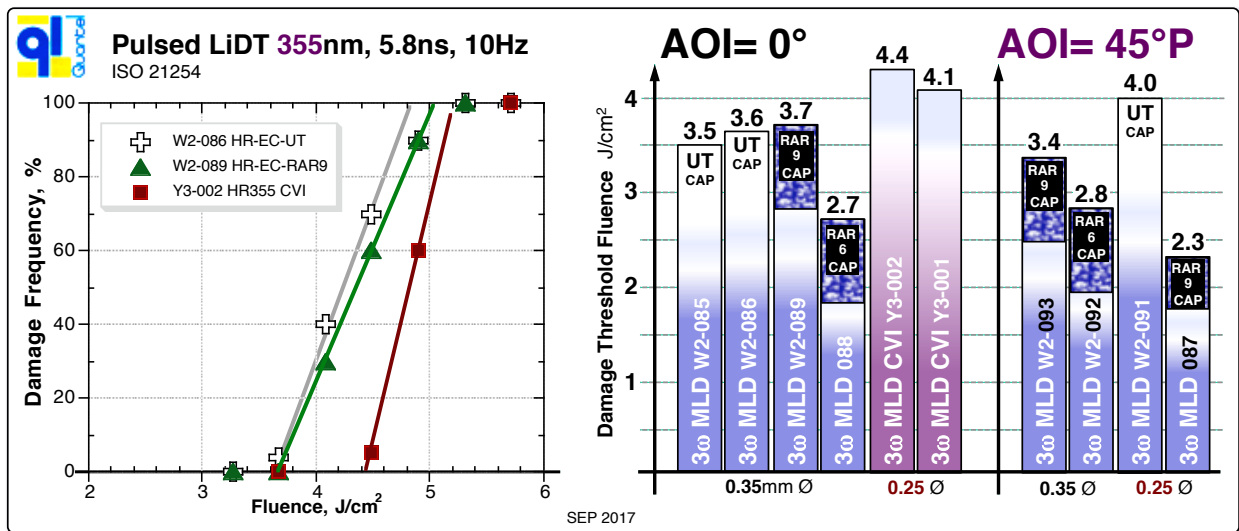


Figure 16: Damage frequency vs. fluence level (left), and a bar chart (right) comparing damage threshold values found for 355nm, 5.8ns pulsed LiDT testing at Quantel of MLD HR film stacks with and without RAR nano-texturing.

## 4.2 Nano-structure array resonant high reflector prototypes

Figure 17 shows pulsed LiDT test results for multiple NSR prototypes, including a control sample with a coating only and no grating structure. The scatter plot (left) plots the frequency of damage vs. fluence on test sites probed with a 0.24mm spot size of 355nm, S-polarized light at 45° AOI. NSR samples underperformed in comparison to the control window with no grating, which is represented by red squares on the plot and had a damage threshold fluence of 4.0 J/cm<sup>2</sup>. The HfO<sub>2</sub> only coated NSR, represented by blue dots on the scatter plot, performed the worst with a damage threshold of only 1.1 J/cm<sup>2</sup>. This may indicate the grating etch process or the irregular growth pattern of the HfO<sub>2</sub> on top of the grating lines, may be degrading the LiDT. NSRs that were coated with both SiO<sub>2</sub> and HfO<sub>2</sub> had similar damage thresholds, but the UT capped NSR suffered damage less frequently than the RAR-textured NSR, when comparing the white cross (UT) and green triangle (RAR) data points.

The bar graph in the right half of the figure shows the linear fit damage threshold fluences at 45° AOI for a 0.24mm exposure area with S-polarized light. All three designs with silica cap layers had similar damage thresholds, suggesting that the HfO<sub>2</sub> layer is likely the greatest contributor to a low damage threshold. This could be attributed to the deposition technique and coating quality, specifically where growth defects can lead to surface absorption. It is also possible that another high-index material, such as aluminum oxide, could be used in place of HfO<sub>2</sub> to raise damage threshold. Further investigations into the effects of grating depth and duty cycle on damage threshold will be made as the NSR design is iterated.

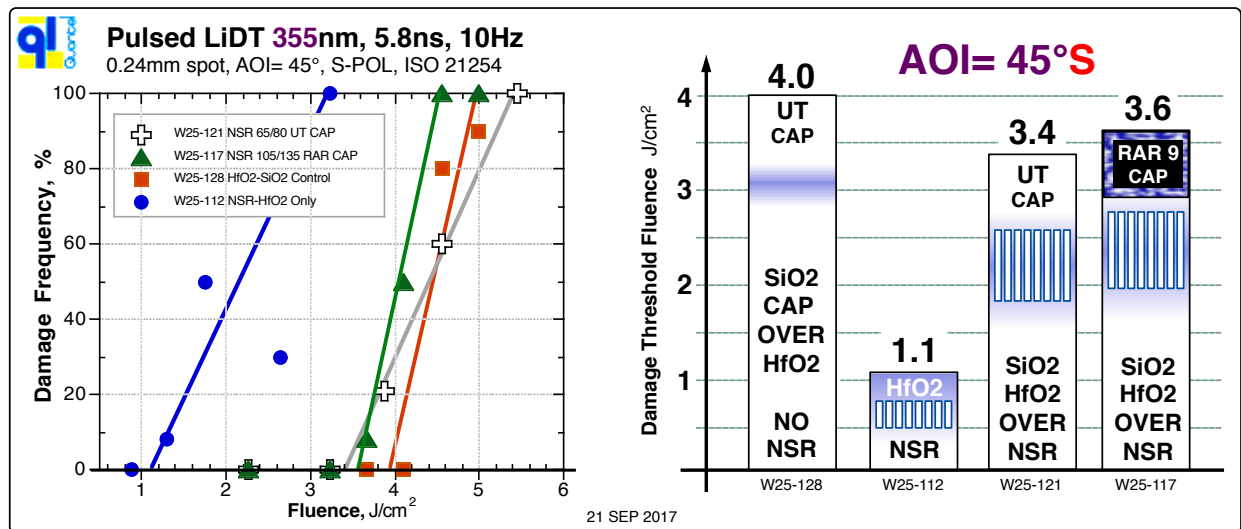


Figure 17: Damage frequency vs. fluence level (left), and a bar chart (right) comparing damage threshold values found for 355nm, 5.8ns pulsed LiDT testing at Quantel of NSR prototypes.

## 5.0 SUMMARY

Pulsed laser damage testing at a 355nm wavelength was completed for two types high reflector optics utilizing nanometer-scale microstructure arrays. Surface absorption scans of RAR nano-texture enhanced MLD HR stacks showed a slight decrease in absorption compared to non-textured MLD HR stacks, however pulsed LiDT testing showed no improvement in damage resistance. Prototype polarization and wavelength selective nano-structure resonant (NSR) array filters were designed and fabricated. Performance of NSR prototypes was limited and not in good agreement with the design models due to multiple fabrication and testing issues. Pulsed LiDT tests of the NSR prototypes showed a threshold in the 3 to 4 J/cm<sup>2</sup> range, comparable to that obtained for the two-layer film stack alone. Further fabrication improvements are needed to realize high performance nano-structure array resonators before the potential for increased laser damage resistance can be evaluated.



## 6.0 ACKNOWLEDGEMENTS

The authors gratefully acknowledge the detailed surface and bulk absorption scans conducted by Chris Franz of Island Interferometry, a spin-out from Stanford PhotoThermal Solutions, Incorporated. Gary Shafer of Quantel USA (GShafer@quantelusa.com) is also gratefully acknowledged for his fast and thorough work providing the certified, NIST traceable pulsed LiDT testing at 355nm. The authors thank Tyler Wozmak & John Knowles at MicroVision Laboratories, Chelmsford MA for the detailed SEM images presented. Last, the authors greatly appreciate the helpful discussions with Karl George Jr. and the exceptional thin film dielectric coating services provided by his company Quality Thin Films, Inc. of Oldsmar Florida USA.

## 7.0 REFERENCES

- [1] Wilson, S.J., and Hutley, M.C., "The optical properties of 'moth eye' antireflection...", *Optica Acta* **29**, (1982)
- [2] Lowdermilk, W. H., Milam, D., "Graded-index antireflection....", *Appl. Physics Letters*, **36** (11), 891 (1980)
- [3] Grann, E. B., et. al., "Optimal design for antireflective tapered.... grating structures," *JOSA A* **12**, 333 (1995)
- [4] Hobbs, D. S., MacLeod, B. D., "High laser damage.... micro-structures..", *Proc. SPIE*, **6720**, 67200L (2007)
- [5] Hobbs, D. S., "Laser damage threshold measurements...near UV ... mid..", *Proc. SPIE*, **7842**, 78421Z (2010)
- [6] Schulze, M., et. al., "Durability of stochastic antireflective structures - .....", *Opt. Exp.* **20** (16), 18348 (2012)
- [7] Hobbs, D. S., et.al., "Contamination resistant antireflection nano-textures..", *Proc. SPIE*, **8885**, 88850J (2013)
- [8] Xin, Y., et. al., "High power laser antireflection subwavelength...", *J. Phys. D: Appl. Phys.* **49**, 265104 (2016)
- [9] Cowan, J. J., "Aztec surface relief volume diffractive structure," *JOSA A* **7**, (8), 1529 (1990)
- [10] Ghiradella, H., "Light and color on... structural colors in butterflies and moths," *Applied Optics* **30**, 0 (1991)
- [11] Tolenis, T., et. al., "Sculptured anti-reflection coatings for high power....", *Opt. Mat. Exp.* **7** (4), 1249 (2017)
- [12] Tolenis, T., et. al., "Next generation .... mirrors ... all-silica layers," *Scientific Reports* **7**, 10898 (2017)
- [13] Hessel, A., and Oliner, A.A., "A New Theory of Wood's Anomal... gratings," *Appl. Opt.* **4** (10), 1275 (1965)
- [14] Mashev, L., and Popov, E., "Zero Order.... of Dielectric Coated Gratings," *Opt. Commun.* **55** (6), 377 (1985)
- [15] Mazuruk, K., "Bragg diffraction in the vicinity of Wood's anomalies," *JOSA A* **7**, (8), 1464 (1990)
- [16] Wang, S.S., and Magnusson, R., "Theory.... Guided-mode resonance filters," *Applied Optics* **32**, 2606 (1993)
- [17] Brundrett, D.L., et. al., "Normal-incidence guided-mode resonant grating filter..", *Opt Lett.* **23** (9), 700 (1998)
- [18] Yu, W., et. al., "Synthesis of polarization-select.... subwavelength structures," *Proc. SPIE*, **5183**, 184 (2003)
- [19] Hobbs, D.S., "Laser-Line Rejection or Transmission Filters... Infrared ...", *Proc. SPIE* **5786**, 578638 (2005)
- [20] Ivanov, M., and Rochon, P., "Polarization-.... resonant .... reflection filter," *Opt. Eng.* **46** (10), 100503 (2007)
- [21] Hobbs, D.S., "Laser Damage Threshold Measurements... High Reflectors," *Proc. SPIE* **7132**, 71321K (2008)
- [22] Pung, A., "High-power laser testing of 3D meta-optics," *Proc. SPIE*, **8885**, 88850K (2013)
- [23] Magnusson, R., "Wideband reflectors with zero-contrast gratings," *Optics Letters* **39**, (15) 4337 (2014)
- [24] Byrd, M.J., et. al., "Blue Laser Diode.... Resonant Mirror," *IEEE Photon. Tech. Lett.* **26** (23), 2311 (2014)
- [25] Yu, W., et. al., "Impacts of tapered sidewall profile.... wideband reflectors," *J. Nano Photon.* **9**, 093058 (2015)
- [26] Chen, G., et. al., "Period photonic filters: theory and experiment," *Opt. Eng.* **55** (3), 037108 (2016)
- [27] Yamada, K., et. al., "Flat-top narrowband filters enabled by guided-mode....", *Opt. Lett.* **42** (20), 4127 (2017)
- [28] Zhang, S., et. al., "Broadband guided-mode resonant reflectors with ....", *Opt. Exp.* **25** (23), 28451 (2017)
- [29] Alexandrovski, A., et. al., "Photothermal common-path interferometry...." *Proc. SPIE* **7193**, 71930D (2009)
- [30] Hobbs, D.S., et. al., "Automated Interference Lithography Systems for .....", *Proc. SPIE* **3879**, 124 (1999)